Molecular Simulation
Vol. 35, No. 7, June 2009, 554–560

Taylor & Francis
Taylor & Francis Group

Dissipative particle dynamics of tension-induced membrane fusion

Andrea Grafmüller[a], Julian Shillcock[b] and Reinhard Lipowsky[a]*

[a]*Theory and Bio-Systems, Max Planck Institute for Colloids and Interfaces, Potsdam, Germany;* [b]*MEMPHYS, University of Southern Denmark, Odense, Denmark*

(*Received 31 October 2008; final version received 8 November 2008*)

Recent studies of tension-induced membrane fusion using dissipative particle dynamics (DPD) simulations are briefly reviewed. The stochastic nature of the fusion process makes it necessary to simulate a large number of fusion attempts in order to obtain reliable fusion statistics and to extract meaningful values for the fusion probability and the average fusion times. All successful fusion events follow the same pathway. In this fusion pathway, configurations of individual lipids play an important role. Fusion starts with individual lipids assuming a splayed tail configuration with one tail inserted into each membrane. In order to determine the corresponding energy barrier, we measure the average work to displace one lipid molecule from one bilayer to the other. This energy barrier is found to depend strongly on a certain DPD parameter, and, thus, can be adjusted in the simulations. Overall, three sub-processes have been identified in the fusion pathway. Their energy barriers are estimated to lie in the range $8-15k_BT$. The fusion probability is found to possess a maximum at intermediate tension values. As one decreases the tension, the fusion probability seems to vanish before the tensionless membrane state is attained. This would imply that the tension has to exceed a certain threshold value in order to induce fusion.

Keywords: membrane fusion; computer simulation; energy barrier; membrane tension; fusion probability

1. Introduction

Fusion of biological membranes is an essential process in many areas of cell biology, ranging from vesicular trafficking and synaptic transmission to cell–cell fusion or viral fusion. Lipid vesicles, which are often used as simplified model systems [1] for the complex biological membranes, can also be induced to fuse experimentally by a variety of methods.

The initial fusion pore is believed to be a neck-like connection with an initial size of about 10 nm. The corresponding time scale has not been measured directly, but experimental evidence suggests that the fusion pore can be formed in less than 100 μs [2,3]. Since it is currently not possible to resolve these length and time scales experimentally, theoretical or computational models are employed to gain insight into the process of fusion pore formation.

Computer simulations such as Brownian Dynamics [4], Monte Carlo simulations [5], coarse-grained molecular dynamics (MD) [6,7,8], dissipative particle dynamics (DPD) [9,10] and atomistic MD [11,12] have been used in recent years to give a molecular picture of the process. These simulation studies observe different fusion pathways and highlight the importance of lipid conformations in the process; but they do not usually allow one to measure the energy barriers between states. A Markovian state model based on coarse-grained MD [13,14] has managed to deduce the energy difference between the initial state and several intermediates from the transition rates.

We have used DPD simulations to probe the statistics of many fusion attempts [15,16]. From the statistics of the fusion time in combination with separate simulations enforcing certain lipid conformations, two energy barriers for fusion could be identified and estimated. These two energy barriers govern (i) the initial flips of lipid molecules from one bilayer to the other and (ii) the nucleation of a small hemifused membrane segment.

We focus on the presumably simplest way to induce lipid bilayer fusion, namely via membrane tension. Our fusion geometry consists of a vesicle with a diameter of 14 or 28 nm in contact with a planar bilayer. To obtain sufficient statistics, the time evolution of over 160 fusion attempts of a vesicle to a planar bilayer patch is monitored. In those simulations, the initial projected area per molecule, A, is varied systematically and serves as a control parameter.

2. Method

DPD is a coarse-grained, particle-based simulation technique that explicitly includes water and reproduces hydrodynamic behaviour [17,18]. The DPD particles or beads represent small volumes of fluid rather than single

*Corresponding author. Email: lipowsky@mpikg.mpg.de

ISSN 0892-7022 print/ISSN 1029-0435 online

DOI: 10.1080/08927020802610296
http://www.informaworld.com

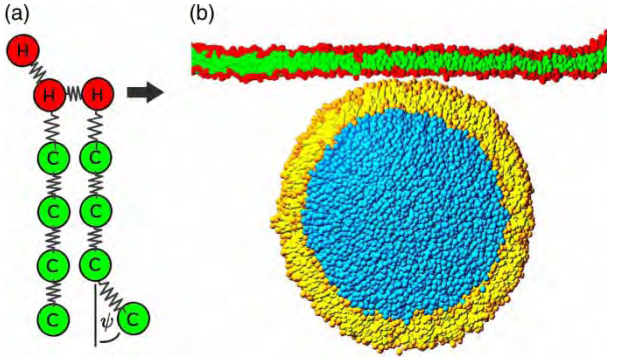

Figure 1. (a) A coarse-grained bead and spring model of DMPC consisting of three head (H) beads and two hydrocarbon chains, each made from four chain (C) beads. Consecutive beads are connected by springs and the hydrophobic chains are stiffened by a three-body potential constraining the angle ψ between two consecutive bonds [21]. (b) Model system consisting of a vesicle with a diameter of 28 nm close to a planar membrane that spans the simulation box with side length $L_{\|} = 50$ nm. The rest of the box is filled with water (W) beads. The water beads outside the vesicle are not shown.

atoms so that their interactions are softly repulsive and short ranged. All interaction potentials have the same range r_0; but their amplitudes a_{ij} differ for different bead species.

More complex molecules, such as the model lipids shown in Figure 1, are constructed by connecting adjacent beads with spring potentials. In addition, hydrocarbon chains are stiffened by a bending potential for two consecutive bonds.

For the simulations, these model lipids are pre-assembled to form a planar membrane and a vesicle

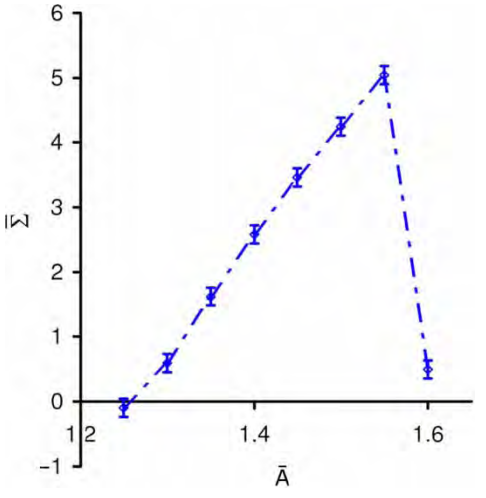

Figure 2. Bilayer tension $\bar{\Sigma}$ as a function of area per molecule $\bar{A}$. Error bars represent the SE. The tension vanishes for $\bar{A}_0 \simeq 1.25$, increases linearly up to $\bar{A} \simeq 1.55$ and then drops abruptly because the membrane ruptures.

Table 1. Amplitudes a_{ij} of the conservative forces between head (H), chain (C) and water (W) beads in units of $k_B T/r_0$. The parameter a_{WW} is chosen to reproduce the compressibility of water. All values of a_{ij} satisfy $a_{ij} \geq 10$ to ensure correct diffusive behaviour [20].

a_{ij}	H	C	W
H	30	35	30
C	35	10	75
W	30	75	25

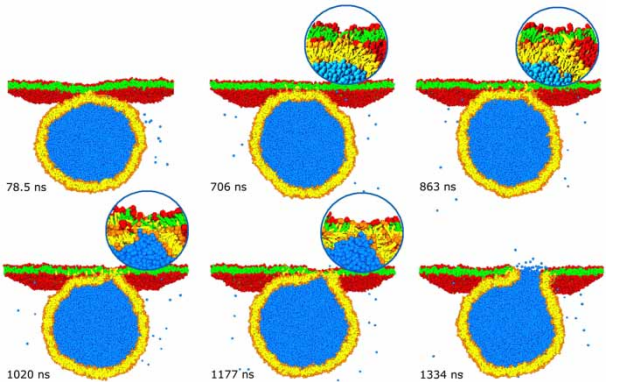

Figure 3. Fusion of a vesicle with a diameter of 28 nm to a planar membrane with a projected area of $(50\,\text{nm})^2$. The vesicle consists of 6869 lipids (orange heads, yellow chains), while the planar membrane contains 6911 lipids (red heads, green chains). The water beads originally inside the vesicle are blue, those outside are not shown for clarity. Six snapshots illustrating the development of the fusion event from 78.5 ns after the first contact until opening of the fusion pore after 1334 ns. The insets are magnifications of the lipid rearrangements at the contact line.

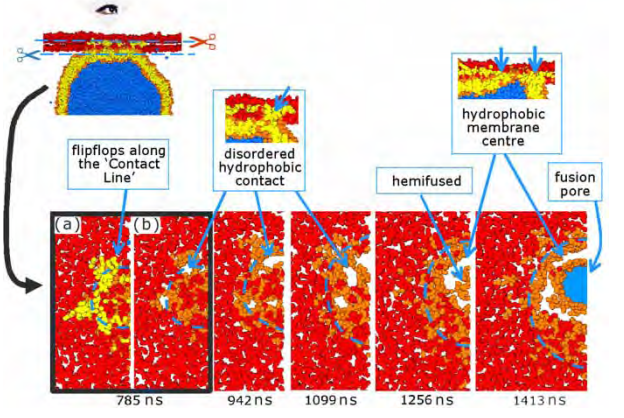

Figure 4. Cross sections of the snapshots shown in Figure 3, cut through the midplane of the planar membrane and viewed from above. The green hydrophobic beads from the planar bilayer are made transparent, so that view (a) of the first snapshot shows the yellow hydrophobic chains of vesicle lipids that have flipped into the planar bilayer. In view (b) of the first snapshot and in the four subsequent snapshots, all hydrophobic beads are made transparent, so that white areas in the head group plane indicate purely hydrophobic regions.

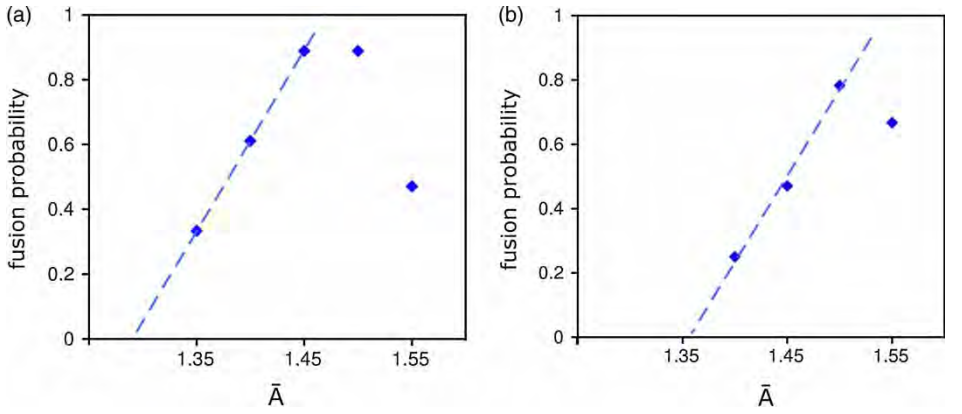

Figure 5. Fusion probability as a function of molecular area $\bar{A}$ for (a) the 14 nm and (b) the 28 nm vesicles. In both cases, the fusion probability, i.e. the fraction of fusion attempts that lead to fusion within 20 μs, exhibits a maximum at $\bar{A}_{\max}$ with $1.45 < \bar{A}_{\max} < 1.5$ in (a) and $\bar{A}_{\max} \simeq 1.5$ in (b) corresponding to the tensions $\bar{\Sigma} \simeq 3.36$ and 4.25, respectively. At higher tensions, fusion becomes less likely because of membrane rupture; at lower tensions, fusion is more and more replaced by hemifusion or adhesion. Linear extrapolation of the data to smaller values of $\bar{A}$ indicates that tensionless membranes will not fuse spontaneously for both systems. The threshold values for the molecular area found from the extrapolation are $\bar{A}_{\text{th}} = 1.29$ and 1.36. The corresponding tension threshold is estimated to be $\bar{\Sigma}_{\text{th}} \simeq 0.56$ for the 14 nm vesicles and $\bar{\Sigma}_{\text{th}} \simeq 1.79$ for the 28 nm vesicles.

separated by a thin water layer, and the rest of the simulation box is filled with water (W) beads. The area of the planar membrane patch is $(72\,r_0)^2 \simeq (50\,\text{nm})^2$, and the diameter of the vesicle is $20\,r_0 \simeq 14\,\text{nm}$ or $40\,r_0 \simeq 28\,\text{nm}$. The simulation parameters are chosen in such a way that the simulated membranes reproduce the experimentally measurable properties of dimyristoylphosphatidylcholine (DMPC) membranes. The force parameters for the three bead species are shown in Table 1.

It is convenient to express properties of the system as dimensionless quantities in units of the bead radius r_0, the energy scale k_BT and the bead mass m_0. These will be indicated by a bar. Thus, we define the dimensionless area per molecule $\bar{A} \equiv A/r_0^2$ and the dimensionless tension $\bar{\Sigma} \equiv \Sigma r_0^2/k_BT$ with corresponding compressibility modulus $\bar{K}_A \equiv K_A r_0^2/k_BT$.

To obtain physical units, the length scale r_0 and time scale $\tau = \sqrt{r_0^2 m_0/k_BT}$ of the system are chosen to match the experimental values for the area per molecule A of a tensionless bilayer and the lateral diffusion coefficient $D_{\|}$ of the lipids.

Fusion is induced by applying a lateral tension to the planar bilayer. The membrane tension is an essentially linear function of the area per molecule $\bar{A}$ as shown in Figure 2. Using this relation, the tension can be controlled by changing the value of A.

To obtain sufficient fusion statistics, more than 160 fusion simulations have been monitored. For each data point corresponding to a particular value of the control parameter, an average over at least 18 independent simulations is taken.

3. Results

3.1 The fusion pathway

In our simulations, all successful fusion attempts involve the same sequence of events. The simulation snapshots shown in Figure 3 are one example for the pathway of a successful fusion event.

Upon first contact, the vesicle adheres to the planar membrane patch. The contact area grows and the vesicle membrane spreads onto the planar membrane, forming a relatively sharp contact angle at the contact line, i.e. the boundary of the contact area. At this 'kink', molecules start to move from the vesicle into the planar bilayer. These 'interbilayer flips' take place mainly at the contact line (see Figure 4) because the higher curvature compresses the lipid tails.

The interbilayer flipping of the lipids disturbs the local double-bilayer structure and leads to the formation of a disordered membrane domain within the contact zone. The hydrophobic tails moving through the head groups bring the hydrophobic centres of the two bilayers into direct contact. Finally, within this disordered hydrophobic-contact region, lipids reorder to form a small hemifused patch, which expands for a short time and finally ruptures at the rim to form the fusion pore.

Additional insight can be gained by looking at these snapshots from a different perspective: Figure 4 shows cuts through the planar membrane viewed from the top. These top views illustrate two features: (i) in view (a) of the first snapshot many such flipped lipids appear along the contact line, whereas only a few yellow tails can be seen in the centre of the contact area; (ii) the white areas, which

correspond to purely hydrophobic regions, do not expand in a radially symmetric manner, but rather following the contact line, and forming a bean-like patch.

3.2 *Fusion probability and alternative pathways*

Fusion is not the only pathway by which the membrane can reduce its tension. Alternatively, tense membranes can rupture or, at lower tensions, the hemifused patch can expand without rupturing, thereby gaining membrane area and relaxing the membrane tension. Furthermore, at low tension, the adhering state of the two bilayers is often stable over the whole simulation period of about 20 μs.

Figure 5 shows the fraction of successful fusion attempts as a function of the area per molecule. Whereas the success rate of fusion is close to 1 for values of $\bar{A} = 1.45$ and 1.50, it decreases steeply for smaller values of $\bar{A}$, as adhesion and hemifusion become more favourable. In both cases, linear extrapolation to small $\bar{A}$ suggests that the fusion probability goes to zero for molecular areas $\bar{A}$ slightly above the relaxed state for both vesicle sizes. Thus, we propose that the system exhibits threshold values $\bar{A}_{\rm th}$ and $\bar{\Sigma}_{\rm th}$ for tension-induced fusion. Inspection of Figure 5 shows that the threshold values for the molecular area are given by $\bar{A}_{\rm th} = 1.29$ and 1.36 and those for the tension by $\bar{\Sigma}_{\rm th} = 0.56$ and 1.79 for the 14 and the 28 nm vesicles, respectively. Close to these threshold values, the fusion probability would vanish as

$$P_{\rm fu} \approx C_A(\bar{A} - \bar{A}_{\rm th}) \approx C_\Sigma(\bar{\Sigma} - \bar{\Sigma}_{\rm th}), \qquad (1)$$

with $C_A \simeq 5.6$ for the 14 nm and $C_A \simeq 5.3$ for the 28 nm vesicle.

Comparison of the two vesicle sizes shows that (i) the small vesicle can fuse at lower values of $\bar{A}$ than the larger one and (ii) at low tensions, the large vesicle remains in the adhered state, whereas the small vesicle typically hemifuses. These differences are related to the relative size of the two vesicle membranes as compared with the planar membrane.

3.3 *Fusion statistics and energy barriers*

3.3.1 *Fusion time distribution*

The tension determines not only the success rates, but also the time scale of fusion. We define the fusion time $t_{\rm fu}$

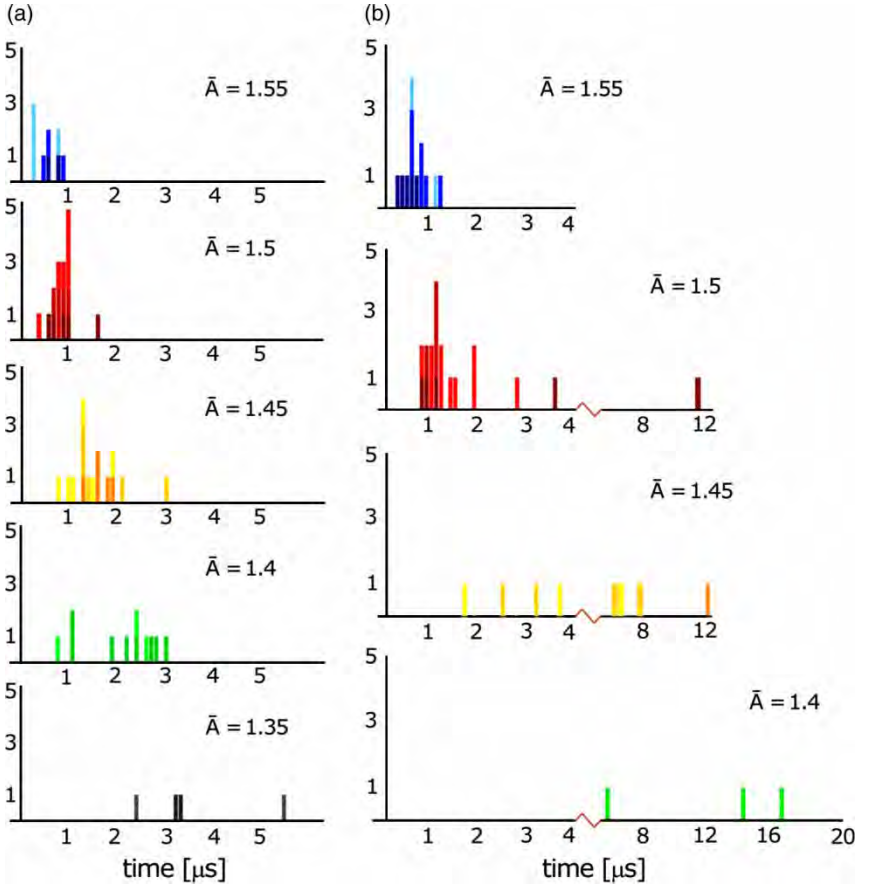

Figure 6. Histograms for the fusion time, $t_{\rm fu}$, (a) for the 14 nm vesicle and (b) for the 28 nm vesicle at different molecular areas $\bar{A}$.

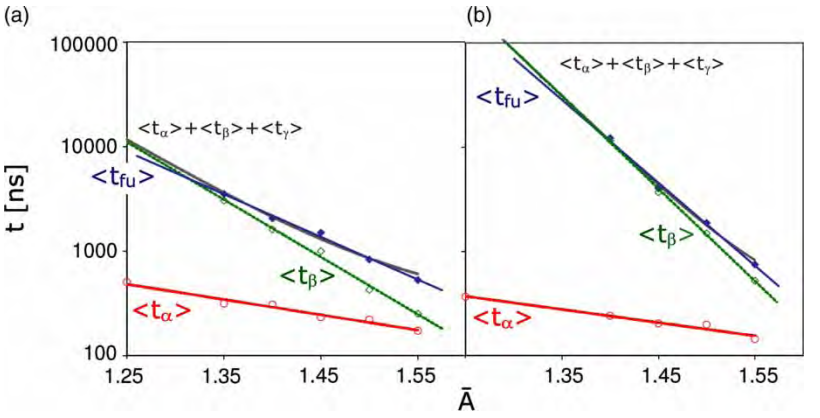

Figure 7. The average duration of the tension-dependent sub-processes $\langle t_\alpha \rangle$ (red circles) and $\langle t_\beta \rangle$ (green diamonds) displayed together with $\langle t_{\mathrm{fu}} \rangle$ (blue diamonds) as a function of the area per molecule $\bar{A}$ (a) for the 14 nm and (b) for the 28 nm vesicle. Both $\langle t_\alpha \rangle$ and $\langle t_\beta \rangle$ show an exponential dependence on $\bar{A}$. The grey curve represents a fit of the fusion time based on the sum $\langle t_\alpha \rangle + \langle t_\beta \rangle + \langle t_\gamma \rangle$, where $\langle t_\gamma \rangle$ is the rupture time of the hemifused diaphragm.

to be the period from first contact between the membranes until the fusion pore has opened. The distributions of fusion times t_{fu} are shown in Figure 6. Inspection of this figure shows that (i) the distributions displayed shift to larger times and (ii) the distributions become wider as the molecular area $\bar{A}$ decreases. In addition, note that the distributions at the different values of $\bar{A}$ overlap considerably, which demonstrates that the results of individual fusion events should not be over-interpreted. To obtain reliable results, or quantitative relations, such as the tension dependence of the fusion times, it is necessary to perform a large number of runs.

Each fusion time distribution, corresponding to a certain value of $\bar{A}$, can be characterised by the average value $\langle t_{\mathrm{fu}} \rangle$, which is shown in Figure 7 as a function of the molecular area $\bar{A}$, and the width $\Delta t_{\mathrm{fu}} \equiv \sqrt{\langle (t_{\mathrm{fu}} - \langle t_{\mathrm{fu}} \rangle)^2 \rangle}$. Both quantities appear to grow exponentially with decreasing $\bar{A}$. This exponential growth of the fusion times together with the decreasing fusion probability as shown in Figure 5 makes it exceedingly difficult to determine the time scale of fusion from computer simulations as the tensionless state is approached.

The tension-dependent fusion times indicate a tension-dependent energy barrier for fusion. In an attempt to identify states that may constitute such a barrier, the fusion process has been decomposed into three sub-processes. (i) Sub-process α corresponds to the first interbilayer flip. The duration of this process defines the first flipping time t_α; (ii) Sub-process β consists of the nucleation of the hemifused patch. The duration of process β, starting from the first interbilayer flip, defines the reordering time t_β; Finally, (iii) sub-process γ corresponds to the rupture of the hemifused patch, which defines the rupture time t_γ. By definition, the total fusion time is given by the sum $t_{\mathrm{fu}} = t_\alpha + t_\beta + t_\gamma$. The average duration of the sub-processes α and β, $\langle t_\alpha \rangle$ and $\langle t_\beta \rangle$, are displayed together with $\langle t_{\mathrm{fu}} \rangle$ as a function of the molecular area in Figure 7. Clearly, both time scales, $\langle t_\alpha \rangle$ and $\langle t_\beta \rangle$, decay exponentially with increasing $\bar{A}$. Their tension dependence can be described by the expressions

$$\langle t_\alpha \rangle = t_{\mathrm{sc}} \exp\left[\Delta \bar{E}_{\alpha,0} - \bar{A}_\alpha \bar{\Sigma}\right], \tag{2}$$

and

$$\langle t_\beta \rangle = t_{\mathrm{sc}} \exp\left[\Delta \bar{E}_{\beta,0} - \bar{A}_\beta \bar{\Sigma}\right]. \tag{3}$$

The third timescale, t_γ, on the other hand, is found to vary between 150 and 300 ns, independent of both tension and vesicle size.

An improved fit of the average fusion time $\langle t_{\mathrm{fu}} \rangle$ thus consists of two superimposed exponentials plus a constant for the rupture time, t_γ, as also shown in Figure 7.

The tension dependence of $\langle t_\alpha \rangle$ and $\langle t_\beta \rangle$ as described by (2) and (3) implies that the corresponding energy barriers should depend linearly on the membrane tension as $\Delta \bar{E}_\alpha = \Delta \bar{E}_{\alpha,0} - \bar{A}_\alpha \bar{\Sigma}$ and $\Delta \bar{E}_\beta = \Delta \bar{E}_{\beta,0} - \bar{A}_\beta \bar{\Sigma}$. Here, $\Delta \bar{E}_{\alpha,0}$ and $\Delta \bar{E}_{\beta,0}$ are the respective barriers for a tension-free membrane and $\bar{A}_\alpha$ and $\bar{A}_\beta$ are characteristic areas. In order to find the values of $\Delta \bar{E}_\alpha$ and $\Delta \bar{E}_\beta$, from extrapolations of the exponential fits in Figure 7, knowledge of the time scale t_{sc} in (2) and (3) is also required. This time scale can be obtained by simulations of enforced flipping as described in the next subsection.

3.3.2 *The flipping sub-process*

Since the sub-process α involves the movement of single lipids, relative to its surroundings, it is accessible to direct simulation. The energy barrier $\Delta \bar{E}_\alpha$ for this process is provided by the (partially) hydrated polar head groups of the proximal monolayers. It is intuitively clear that this

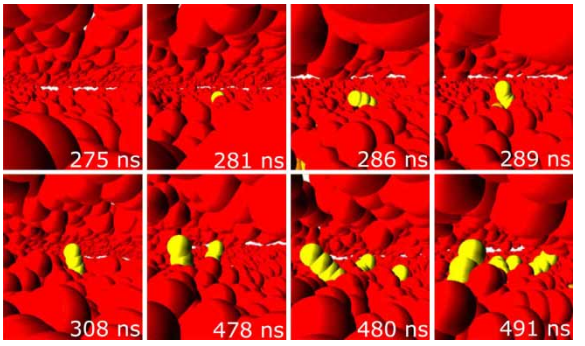

Figure 8. First, interbilayer flips of hydrophobic chains from the vesicle (yellow) into the planar bilayer (head beads red, chain beads not shown). Snapshots of the centre of the planar membrane, with its hydrophobic chains made transparent, so that the first hydrophobic chains from the vesicle (yellow) moving into the planar bilayer become visible.

barrier should decrease with increasing tension Σ, as the tension causes the head groups in the planar membrane to move further apart and thus makes it easier for the hydrophobic chains to cross from one bilayer to the other.

A closer look at the initial flipping events during sub-process α reveals that at first only single lipid tails move to the planar bilayer so that the lipids assume a splayed conformation (Figure 8). To measure the energy barrier for this process, additional simulations have been performed, as illustrated in Figure 9. For two adhering membranes, a single lipid tail is pulled slowly with a harmonic potential from its original position into the other bilayer, so that the lipid has one tail in each bilayer as observed in the fusion simulations. The average work required for this process in 20 independent simulations was found to be $\langle W \rangle = 9 \pm 2k_BT$. This value constitutes an upper limit for the energy barrier $\Delta\bar{E}_{\alpha,0}$ and should correspond to the barrier itself for very slow pulling.

Another estimate for the energy barrier comes from the Jarzynski relation [21], which leads to

$$\exp\left[-\frac{\Delta\mathcal{F}}{k_BT}\right] = \left\langle \exp\left[\frac{-W}{k_BT}\right] \right\rangle. \tag{4}$$

This equality should hold irrespective of how fast the process happens, if a sufficiently large number of trajectories are sampled. The average value:

$$\left\langle \exp\left[\frac{-W_\alpha}{k_BT}\right] \right\rangle,$$

again obtained from the 20 independent enforced flipping simulations, gives a barrier height of $8k_BT$.

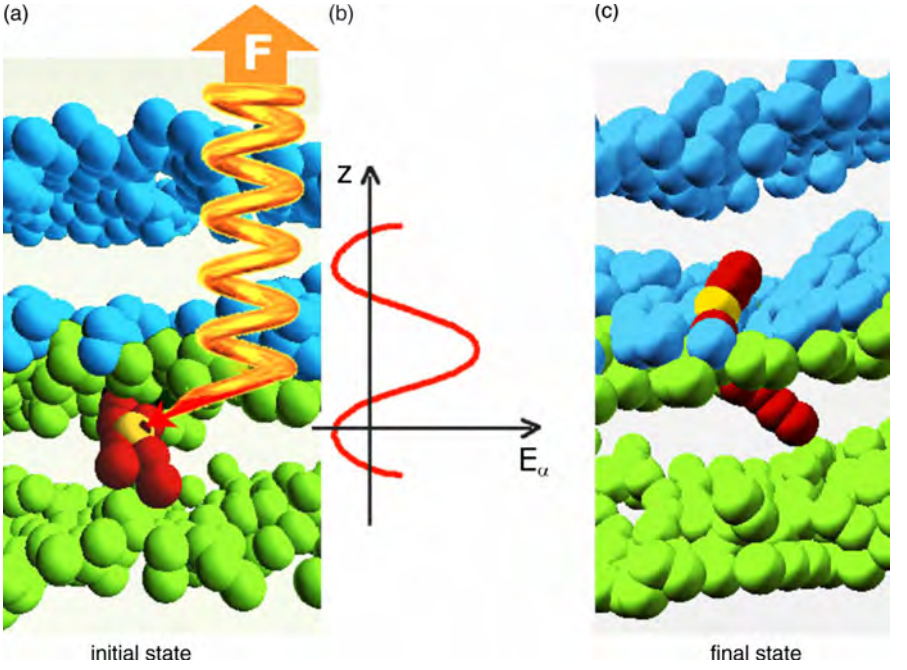

Figure 9. Simulations of enforced lipid flips used to measure the energy barrier $\Delta\bar{E}_\alpha$ (a). From two adhering bilayers (head beads blue/green, tail beads omitted for clarity), a single lipid is selected (orange heads, yellow/red tails) and a force F arising from a slowly moving harmonic potential is applied to one of its tail beads (yellow), until the tail flips to the other bilayer, so that the lipid assumes a splayed configuration with one tail inserted into each bilayer as shown in (c). (b) Energy landscape E_α for the bead as a function of the displacement z of the yellow bead. It has a high barrier in the centre corresponding to the repulsive head groups and increases to the sides reflecting displacement of the head group into the hydrophobic region.

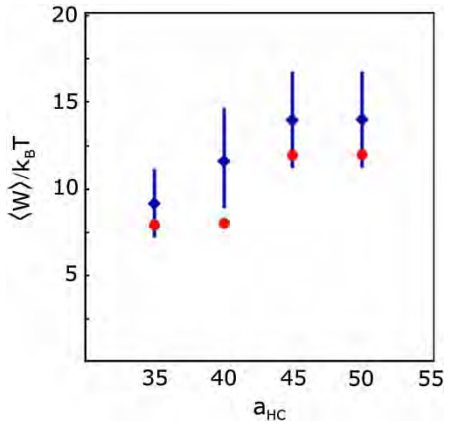

Figure 10. Average work $\langle W \rangle$ required to enforce an interbilayer flip as a function of the force amplitude a_{HC} acting between H and C beads. Diamonds: direct measurement of the average work. Error bars represent one SD. Circles: average work determined by the Jarzynski equation (4). In both cases the average was calculated from 20 independent simulations.

The energy barrier $\Delta\bar{E}_\alpha$, which arises from hydration in real membranes, is implemented in the coarse-grained simulations via the stronger force amplitude a_{HC} between head (H) and tail (C) beads. Therefore, for a given lipid architecture and parameter set, the height of the barrier can be expected to be primarily governed by the value of the a_{HC}.

This expectation is confirmed by simulations of enforced interbilayer flips using different values of the a_{HC} parameter in the range $a_{HC} = 35–50$ as shown in Figure 10.

Since the flipping barrier depends on a_{HC}, its magnitude can be tuned in such a way that the energy barrier is consistent with available reference data. A possible experimental estimate of the barrier height can be deduced from the hydration energy of one hydrocarbon chain, which can be estimated from the critical micelle concentration. For DMPC this is of the order of $10k_BT$.

3.3.3 *The total energy barrier*

Since the energy barrier for one of the sub-processes of fusion could be measured in independent simulations, the time scale t_{sc} has become accessible. Using the same value for t_{sc} in relation (3), the energy barrier $\Delta\bar{E}_{\beta,0}$ for sub-process β at $\bar{\Sigma} = 0$ can be estimated to be $\Delta\bar{E}_{\beta,0} = 11.1 \pm 2k_BT$ and $\Delta\bar{E}_{\beta,0} = 14.4 \pm 2k_BT$ for the 14 and 28 nm vesicle, respectively, the barrier for sub-process γ is estimated as $8k_BT$.

At low tensions the total fusion time t_{fu} is dominated by the reordering time, $\langle t_\beta \rangle$ (see Figure 7). Thus, the simulation statistics presented here suggest that the main energy barrier for fusion of tensionless bilayers comes from the reordering process and is of the order of $10–15k_BT$.

References

[1] L.K. Tamm, J. Crane, and V. Kiessling, *Membrane fusion: a structural perspective on the interplay of lipids and proteins*, Curr. Opin. Struct. Biol. 13 (2003), pp. 453–466.

[2] C. Haluska, V. Marchi-Artzner, J. Brienne, J.M. Lehn, R. Lipowsky, and R. Dimova, *Fusion of functionalized giant vesicles*, Biophys. J. 88 (2005), pp. 66A–66A.

[3] M. Lindau and G.A. de Toledo, *The fusion pore*, Biochim. Biophys. Acta – Mol. Cell Res. 1641 (2003), pp. 167–173.

[4] H. Noguchi and M. Takasu, *Fusion pathways of vesicles: a Brownian dynamics simulation*, J. Chem. Phys. 115 (2001), pp. 9547–9551.

[5] M. Müller, K. Katsov, and M. Schick, *New mechanism of membrane fusion*, J. Chem. Phys. 116 (2002), pp. 2342–2345.

[6] S. Marrink and A. Mark, *Mechanism of vesicle fusion as revealed by molecular dynamics simulations*, J. Am. Chem. Soc. 125 (2003), pp. 11144–11145.

[7] M.J. Stevens, J.H. Hoh, and T.B. Woolf, *Insights into the molecular mechanism of membrane fusion from simulation: evidence for the association of splayed tails*, Phys. Rev. Lett. 91 (2003), 188102.

[8] A.F. Smeijers, A.J. Markvoort, K. Pieterse, and A.J. Hilbers, *A detailed look at vesicle fusion*, J. Phys. Chem. B 110 (2006), pp. 13212–13219.

[9] J. Shillcock and R. Lipowsky, *Tension-induced fusion of bilayer membranes and vesicles*, Nat. Mater. 4 (2005), pp. 225–228.

[10] D.W. Li and X.Y. Liu, *Examination of membrane fusion by dissipative particle dynamics simulation and comparison with continuum elastic models*, J. Chem. Phys. 122 (2005), pp. 1749091–1749098.

[11] V. Knecht, A.E. Mark, and S.J. Marrink, *Phase behavior of a phospholipid/fatty acid/water mixture studied in atomic detail*, J. Am. Chem. Soc. 128 (2006), pp. 2030–2034.

[12] V. Knecht, A.E. Mark, and S.J. Marrink, *Molecular dynamics simulations of lipid vesicle fusion in atomic detail*, Biophys. J. 92 (2007), pp. 4254–4261.

[13] P.M. Kasson, N.W. Kelley, N. Singhal, M. Vrljic, A.T. Brunger, and V.S. Pande, *Ensemble molecular dynamics yields submillisecond kinetics and intermediates of membrane fusion*, Proc. Natl. Acad. Sci. USA 103 (2006), pp. 11916–11921.

[14] P.M. Kasson, A. Zornorodian, S. Park, N. Singhal, L.J. Guibas, and V.S. Pande, *Persistent voids: a new structural metric for membrane fusion*, Bioinformatics 23 (2007), pp. 1753–1759.

[15] A. Grafmüller, J. Shillcock, and R. Lipowsky, *Pathway of membrane fusion with two tension-dependent energy barriers*, Phys. Rev. Lett. 98 (2007), 218101.

[16] A. Grafmüller, J. Shillcock, and R. Lipowsky, *The fusion of membranes and vesicles-pathway and energy barriers from dissipative particle dynamics*, Biophys. J. (2009), in press.

[17] R.D. Groot and P.B. Warren, *Dissipative particle dynamics: bridging the gap between atomistic and mesoscopic simulation*, J. Chem. Phys. 107 (1997), pp. 4423–4435.

[18] I. Vattulainen, M. Karttunen, G. Besold, and J.M. Polson, *Integration schemes for dissipative particle dynamics simulations: from softly interacting systems towards hybrid models*, J. Chem. Phys. 116 (2002), pp. 3967–3979.

[19] C. Jarzynski, *Nonequilibrium equality for free energy differences*, Phys. Rev. Lett. 78 (1997), pp. 2690–2693.

[20] S.D. Stoyanov and R.D. Groot, *From molecular dynamics to hydrodynamics: a novel Galilean invariant thermostat*, J. Chem. Phys. 122 (2004), pp. 114112/1–114112/8.

[21] R. Goetz and R. Lipowsky, *Computer simulations of bilayer membranes: self-assembly and interfacial tension*, J. Chem. Phys. 108 (1998), pp. 7397–7409.